

Robust Data-Enabled Predictive Leading Cruise Control via Reachability Analysis

1st Shuai Li

*School of Vehicle and Mobility
Tsinghua University
Beijing, China
li-s21@mails.tsinghua.edu.cn*

2nd Chaoyi Chen

*School of Vehicle and Mobility
Tsinghua University
Beijing, China
chency2023@tsinghua.edu.cn*

3rd Haotian Zheng

*School of Vehicle and Mobility
Tsinghua University
Beijing, China
zhenght21@mails.tsinghua.edu.cn*

4th Jiawei Wang

*School of Vehicle and Mobility
Tsinghua University
Beijing, China
wang-jw18@tsinghua.org.cn*

5th Qing Xu

*School of Vehicle and Mobility
Tsinghua University
Beijing, China
qingxu@tsinghua.edu.cn*

6th Keqiang Li

*School of Vehicle and Mobility
Tsinghua University
Beijing, China
likq@tsinghua.edu.cn*

Abstract—Data-driven predictive control promises model-free wave-dampening strategies for Connected and Autonomous Vehicles (CAVs) in mixed traffic flow. However, its performance relies on data quality, which suffers from unknown noise and disturbances. This paper introduces a Robust Data-Enabled Predictive Leading Cruise Control (RD_{ee}P-LCC) method based on reachability analysis, aiming to achieve safe and optimal CAV control under bounded process noise and external disturbances. Precisely, the matrix zonotope set technique and Willems’ Fundamental Lemma are employed to derive the over-approximated system dynamics directly from data, and a data-driven feedback control technique is utilized to obtain an additional feedback input for stability. We decouple the mixed platoon into an error system and a nominal system, where the error system provides data-driven reachability sets for the enhanced safety constraints in the nominal system. Finally, a data-driven predictive control framework is formulated in a tube-based control manner for robustness guarantees. Nonlinear simulations with noise-corrupted data demonstrate that the proposed method outperforms baseline methods in mitigating traffic waves.

Index Terms—data-driven predictive control, connected and autonomous vehicles, mixed traffic

I. INTRODUCTION

Platooning technologies involving multiple Connected and Autonomous Vehicles (CAVs) have experienced rapid development [1]. By exploiting the benefits of vehicle-to-vehicle communications and cooperative control algorithms, significant improvements have been achieved in traffic safety, energy economy, and driving comfort for pure CAV platoons [2]. However, the full marketization of CAVs is an evolving process. A mixed traffic scenario will persist during this transitional period, characterized by the coexistence of CAVs and Human-Driven Vehicles (HDVs) [3], [4].

This work is supported by National Natural Science Foundation of China under grant 52302410, Postdoctoral Fellowship Program of CPSF under grant GZB20230354, Tsinghua University-Huawei Joint Research Project, Young Elite Scientists Sponsorship Program by CHINA-SAE, and Shuimu Tsinghua Scholarship. Corresponding author: Jiawei Wang and Keqiang Li.

Unlike pure CAV platoons, mixed platoons incorporating CAVs and HDVs do not require all vehicles to have autonomous driving capabilities, making them directly applicable to mixed traffic. By appropriate design of CAV cooperation strategies, recent research has revealed the potential of mixed platoons in attenuating undesired traffic perturbations and smoothing traffic flow [5], [6]. Existing research mostly captures the HDVs’ dynamics by a car-following model and employs model-based control methods for the CAVs. These methods include optimal control [7], Model Predictive Control (MPC) [8], and control barrier function [9]. However, their performance relies heavily on the model accuracy, while in practice, the HDVs’ dynamics are usually unknown and uncertain. In contrast, model-free methods, which bypass the need for prior knowledge of mixed platoon dynamics, have recently shown their potential in learning CAV control policies from data, as evidenced by techniques such as adaptive dynamic programming [10] and reinforcement learning [5]. Nevertheless, these methods typically require iterative approximations to find optimal solutions, which can significantly increase computational demands. Also, their lack of guaranteed safety and interpretability limits their practical implementations.

On the other hand, combining data-driven methods and the well-established MPC, data-driven predictive control promises safe and optimal controllers from data [11]. One notable technique is Data-Enabled Predictive Control (DeePC) [12], which utilizes Willems’ fundamental lemma [13] to represent the behavior of unknown systems in a data-centric manner. By adapting DeePC to a Leading Cruise Control (LCC) framework [6], the recently introduced Data-Enabled Predictive Leading Cruise Control (DeeP-LCC) allows for CAVs’ optimal cooperation in mixed platoons from measurable traffic data with explicit safety constraints [14]. Both nonlinear traffic simulations [14] and real-world experiments [15] have validated its wave-dampening capability without requiring

knowledge of surrounding HDVs' car-following dynamics. However, existing research has overlooked the noise impact on offline data collection and online predictive control, and imposes over-simplified assumptions for external disturbances, which could still raise safety concerns [16]. Indeed, emerging evidence has suggested that robustifying standard DeePC could significantly enhance its safety performance [17], [18]. Along this direction, a very recent paper has reformulated DeeP-LCC by min-max robust optimization to tackle unknown disturbances on the head vehicle [19], but the noise issue for the overall traffic has not been well addressed.

Compared to min-max reformulation, reachability analysis provides a computationally more reliable technique for robustness against all possible noise and disturbances. Recent studies have utilized this technique to design robust control strategies for CAVs; see, *e.g.*, safety controller synthesis via backward reachability analysis [20] and anti-adversary control using reach-avoid specification [21]. Note that these works are mostly model-based, with one very recent exception in [22], whose prediction accuracy, however, is constrained due to the absence of a data-driven dynamics model.

To address the aforementioned issues, this paper proposes a Robust Data-Enabled Predictive Leading Cruise Control (RDDeP-LCC) method via data-driven reachability analysis, aiming to design robust control strategies for CAVs against unknown noise and disturbances. Our contributions include: 1) We decouple the original mixed platoon system into an idealized nominal system and an error system with bounded noise and disturbances. Inspired by [22], [23], the data-driven reachable sets are calculated for the error system by modeling the system dynamics as an over-approximated matrix zonotope set, and an additional data-driven feedback control law is designed for stability. Similarly to a tube-based MPC mechanism, the reachable sets of the error system are utilized to tighten the safety constraints for the nominal system. Then, a data-driven predictive control formulation is proposed with this enhanced constraint, which, combined with the feedback control law of the error system, provides the CAVs' control inputs with robustness guarantees. 2) Nonlinear simulations with noise-corrupted data and disturbances validate the performance of RDDeP-LCC in mitigating traffic waves and tracking the equilibrium state. In a series of 20 tests with randomly generated offline datasets, RDDeP-LCC consistently demonstrates superior robustness compared to the standard DeeP-LCC [14] or MPC with prior dynamics knowledge.

The rest of this paper is organized as follows. Section II provides preliminaries and system modeling. Section III introduces the RDDeP-LCC method. Section IV shows numerical simulations, and Section V concludes this paper.

II. PRELIMINARIES AND SYSTEM MODELING

In this section, we present some preliminaries and the parametric modeling of the mixed platoon system.

A. Preliminaries

Definition 1 (Zonotope Set [24]): Given a center vector $c_Z \in \mathbb{R}^n$, and $\gamma_Z \in \mathbb{N}$ generator vectors in a generator matrix $G_Z = [g_Z^{(1)}, g_Z^{(2)}, \dots, g_Z^{(\gamma_Z)}] \in \mathbb{R}^{n \times \gamma_Z}$, a zonotope set is defined as $Z = \langle c_Z, G_Z \rangle = \{x \in \mathbb{R}^n \mid x = c_Z + \sum_{i=1}^{\gamma_Z} \beta^{(i)} g_Z^{(i)}, -1 \leq \beta^{(i)} \leq 1\}$. For zonotope sets, the following operations hold:

- **Linear Map:** For a zonotope set $Z = \langle c_Z, G_Z \rangle$, $L \in \mathbb{R}^{m \times n}$, the linear map is defined as $LZ = \langle Lc_Z, LG_Z \rangle$.
- **Minkowski Sum:** Given two zonotope sets $Z_1 = \langle c_{Z_1}, G_{Z_1} \rangle$ and $Z_2 = \langle c_{Z_2}, G_{Z_2} \rangle$ with compatible dimensions, the Minkowski sum is defined as $Z_1 + Z_2 = \langle c_{Z_1} + c_{Z_2}, [G_{Z_1}, G_{Z_2}] \rangle$.
- **Cartesian Product:** Given two zonotope sets $Z_1 = \langle c_{Z_1}, G_{Z_1} \rangle$ and $Z_2 = \langle c_{Z_2}, G_{Z_2} \rangle$, the cartesian product is defined as

$$Z_1 \times Z_2 = \left\langle \begin{bmatrix} c_{Z_1} \\ c_{Z_2} \end{bmatrix}, \begin{bmatrix} G_{Z_1} & 0 \\ 0 & G_{Z_2} \end{bmatrix} \right\rangle.$$

Definition 2 (Matrix Zonotope Set [24]): Given a center matrix $C_M \in \mathbb{R}^{n \times m}$, and $\gamma_M \in \mathbb{N}$ generator matrices in a generator matrix $G_M = [g_M^{(1)}, g_M^{(2)}, \dots, g_M^{(\gamma_M)}] \in \mathbb{R}^{n \times m \gamma_M}$, a matrix zonotope set is defined as $M = \langle C_M, G_M \rangle = \{X \in \mathbb{R}^{n \times m} \mid X = C_M + \sum_{i=1}^{\gamma_M} \beta^{(i)} G_M^{(i)}, -1 \leq \beta^{(i)} \leq 1\}$.

Definition 3 (Persistently excitation [13]): Given a signal sequence $\omega = \text{col}(\omega(1), \omega(2), \dots, \omega(T))$ of length $T \in \mathbb{N}^1$, the sequence ω is persistently exciting with order $l \in \mathbb{N}$ if and only if the following Hankel matrix is of full row rank:

$$\mathcal{H}_l(\omega) = \begin{bmatrix} \omega(1) & \omega(2) & \cdots & \omega(T-l+1) \\ \omega(2) & \omega(3) & \cdots & \omega(T-l+2) \\ \vdots & \vdots & \ddots & \vdots \\ \omega(l) & \omega(l+1) & \cdots & \omega(T) \end{bmatrix}. \quad (1)$$

Lemma 1 (Willems' Fundamental Lemma [13]): Consider a controllable Linear Time-Invariant (LTI) system. Let $u^d = \text{col}(u(1), u(2), \dots, u(T))$ be an input sequence persistently exciting with order $L + n$, where n is the dimension of the system state, and the corresponding state sequence is $x^d = \text{col}(x(1), x(2), \dots, x(T))$. Then u^s and x^s is a length- L input-output trajectory of the system if and only if there exists a vector $g \in \mathbb{R}^{T-L+1}$ satisfying

$$\begin{bmatrix} \mathcal{H}_L(u^d) \\ \mathcal{H}_L(x^d) \end{bmatrix} g = \begin{bmatrix} u^s \\ x^s \end{bmatrix}. \quad (2)$$

The physical interpretation of Lemma 1 is that for a controllable LTI system, the subspace consisting of all feasible trajectories (u^s, x^s) of length L is identical to the space spanned by a Hankel matrix of order L constructed from pre-collected data (u^d, x^d) with rich enough control inputs.

¹Given vectors or matrices X_0, X_1, \dots, X_n with compatible sizes, we denote $\text{col}(X_0, X_1, \dots, X_n) = [X_0^\top, X_1^\top, \dots, X_n^\top]^\top$.

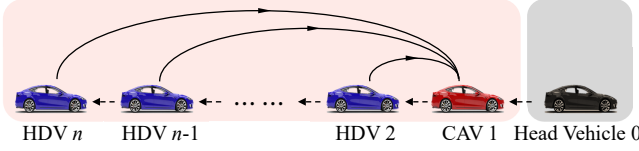


Fig. 1. Schematic for a CF-LCC mixed platoon. The platoon consists of one leading CAV (colored in red) and multiple following HDVs (colored in blue), with one head vehicle (colored in black) at the very beginning.

B. Parametric Modeling of Mixed Platoon System

As depicted in Fig. 1, we analyze a mixed platoon system comprising one head vehicle (indexed as 0), one leading CAV (indexed as 1), and $n-1$ following HDVs (indexed as $2, \dots, n$ against the moving direction). This kind of system is called as Car-Following Leading Cruise Control (CF-LCC) in [6], and practical mixed traffic can be naturally partitioned into several CF-LCC systems. Define $\Omega = \{0, 1, 2, \dots, n\}$ as the vehicles' index set.

In the following, we present the common parametric modeling process for the mixed platoons. For all the vehicles $i \in \Omega$, a typical second-order linear longitudinal dynamics [3], [7] are utilized, given by:

$$\begin{cases} \dot{p}_i(t) = v_i(t), \\ \dot{v}_i(t) = u_i(t), \end{cases} \quad (3)$$

where $u_i(t)$ represents the control input, and $p_i(t)$ and $v_i(t)$ represent the position and velocity, respectively.

For HDVs, the control input $u_i(t)$ is determined by the drivers, and can be represented by well-established car-following models like Optimal Velocity Model (OVM) [25], with the general form given by:

$$u_i(t) = F(s_i(t), \dot{s}_i(t), v_i(t)), \quad (4)$$

where $s_i(t) = p_{i-1}(t) - p_i(t)$ and $\dot{s}_i(t) = v_{i-1}(t) - v_i(t)$ denote the spacing and relative velocity between vehicle i and its preceding vehicle, respectively. For simplicity, a homogeneous expression of F is utilized for parametric modeling in this section, but the proposed data-driven control method in this paper is directly applicable to general heterogeneous cases.

Define $\tilde{s}_i(t)$ and $\tilde{v}_i(t)$ as the deviations of spacing and velocity from the equilibrium state, respectively:

$$\tilde{s}_i(t) = s_i(t) - s^*, \quad \tilde{v}_i(t) = v_i(t) - v^*, \quad (5)$$

where s^* and v^* denote the spacing and velocity in traffic equilibrium, satisfying the condition $F(s^*, 0, v^*) = 0$.

Then, the first-order Taylor expansion can be applied to (4), which, combined with (3), yields the HDVs' linearized model:

$$\begin{cases} \dot{\tilde{s}}_i(t) = \tilde{v}_{i-1}(t) - \tilde{v}_i(t), \\ \dot{\tilde{v}}_i(t) = \gamma_1 \tilde{s}_i(t) + \gamma_2 \tilde{v}_i(t) + \gamma_3 \tilde{v}_{i-1}(t), \end{cases} \quad (6)$$

where $\gamma_1 = \frac{\partial F}{\partial s}$, $\gamma_2 = \frac{\partial F}{\partial \dot{s}} - \frac{\partial F}{\partial v}$, and $\gamma_3 = \frac{\partial F}{\partial \dot{s}}$ are evaluated at the equilibrium state (s^*, v^*) .

For the CAV, its linearized longitudinal dynamics can be given in the following form:

$$\begin{cases} \dot{\tilde{s}}_i(t) = \tilde{v}_{i-1}(t) - \tilde{v}_i(t), \\ \dot{\tilde{v}}_i(t) = u_i(t), \end{cases} \quad (7)$$

where $u_i(t)$ is the designed control input for the CAV.

We define $x_i(t) = [\tilde{s}_i(t), \tilde{v}_i(t)]^\top$ as the state vector for vehicle i , and lump all the states of the HDVs and CAV to obtain the mixed platoon system state $x(t) = [x_1(t), x_2(t), \dots, x_n(t)]^\top \in \mathbb{R}^{2n \times 1}$. Then, the state-space model of the mixed platoon is obtained as:

$$\dot{x}(t) = A_{\text{con}}x(t) + B_{\text{con}}u(t) + H_{\text{con}}\epsilon(t) + w(t), \quad (8)$$

where $A_{\text{con}} \in \mathbb{R}^{2n \times 2n}$, $B_{\text{con}} \in \mathbb{R}^{2n \times 1}$, $H_{\text{con}} \in \mathbb{R}^{2n \times 1}$ represent the dynamics matrix, the control input matrix, and the disturbance input matrix, respectively, and $u(t) \in \mathbb{R}$, $\epsilon(t) = \tilde{v}_0(t) \in \mathbb{R}$, $w(t) \in \mathbb{R}^{2n \times 1}$ denote the control input of CAV, the velocity deviation of the head vehicle (external disturbance), and the unknown but bounded process noise, respectively.

Then, one can discretize the continuous system (8) using the forward Euler method to obtain the discrete system model:

$$x(k+1) = Ax(k) + Bu(k) + H\epsilon(k) + w(k), \quad (9)$$

where k is the discrete time step, A , B , and H are system matrix, control input matrix, disturbance input matrix of the discrete system, respectively.

Remark 1: It is worth noting that the uncertain and unknown nature of HDVs' behaviors makes it non-trivial to accurately identify the parametric model (9), which motivates us to develop a data-driven predictive control method. We present the general form of model (9) to facilitate our following design of the data-driven dynamics and reachability analysis, and it will also be utilized for the baseline MPC method in the simulations. Due to the page limit, interested readers are referred to [6] for the specific expressions of the parametric model.

III. METHODOLOGY OF RDEEP-LCC

This section proposes the RDeeP-LCC method for mixed platoon control, consisting of three steps: data collection, data-driven reachable set computation, and RDeeP-LCC optimization formulation.

Fig. 2 demonstrates the flow chart of the proposed method. In the offline phase (blue), pre-collected data (yellow) is utilized to calculate the over-approximated system matrix \mathcal{M}_{ABH} (blue, center), derive a probabilistic guaranteed feedback control law K to ensure stability for all possible systems (blue, left), and generate the Hankel matrices (blue, right). In the online phase (pink), RDeeP-LCC solves for optimal control input for the CAV in a receding horizon manner. First, based on \mathcal{M}_{ABH} and K , the method recursively derives the data-driven reachable sets of error states (pink, top left), which is further converted into a tightened nominal system constraint (pink, center left). Then, the nominal control input is obtained from the RDeeP-LCC optimization formulation (pink, right).

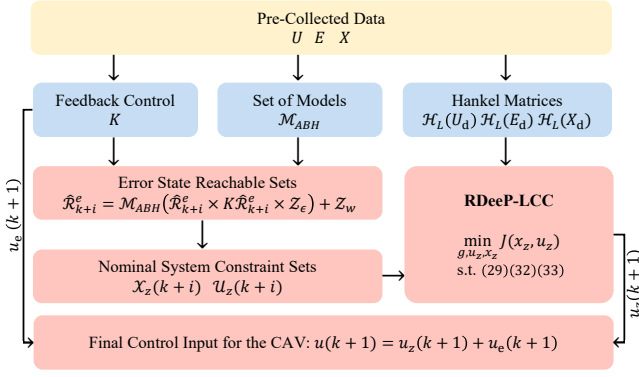


Fig. 2. An overview of the proposed RDdeP-LCC method.

Finally, the actual control input of the CAV is obtained by combining the nominal control input with the error feedback control input using the tube-based MPC mechanism to ensure robustness property (pink, bottom).

A. Data Collection

For data collection, a persistently exciting sequence $u(k)$ and $\epsilon(k)$ of length $T+1$ is needed to be applied to the mixed platoon system. Specifically, define the control input sequence U , the disturbance input sequence E , and the corresponding state sequence X as follows:

$$U = [u(1), u(2), \dots, u(T+1)] \in \mathbb{R}^{1 \times (T+1)}, \quad (10a)$$

$$E = [\epsilon(1), \epsilon(2), \dots, \epsilon(T+1)] \in \mathbb{R}^{1 \times (T+1)}, \quad (10b)$$

$$X = [x(1), x(2), \dots, x(T+1)] \in \mathbb{R}^{2n \times (T+1)}. \quad (10c)$$

For the reachable set computation, the data sequences are further reorganized into a specific format:

$$U_- = [u(1), u(2), \dots, u(T)] \in \mathbb{R}^{1 \times T}, \quad (11a)$$

$$E_- = [\epsilon(1), \epsilon(2), \dots, \epsilon(T)] \in \mathbb{R}^{1 \times T}, \quad (11b)$$

$$X_- = [x(1), x(2), \dots, x(T)] \in \mathbb{R}^{2n \times T}, \quad (11c)$$

$$X_+ = [x(2), x(3), \dots, x(T+1)] \in \mathbb{R}^{2n \times T}. \quad (11d)$$

In addition, for convenience in the subsequent derivation, we denote the sequence of unknown process noise as

$$W_- = [w(1), w(2), \dots, w(T)] \in \mathbb{R}^{2n \times T}, \quad (12)$$

although it is worth noting that W_- is not measurable.

In addition, we reformulate the trajectory data U_- , E_- , and X_- into a compact form as the following column vectors:

$$U_d = \text{col}(U_-) \in \mathbb{R}^T, \quad (13a)$$

$$E_d = \text{col}(E_-) \in \mathbb{R}^T, \quad (13b)$$

$$X_d = \text{col}(X_-) \in \mathbb{R}^{2nT}. \quad (13c)$$

Then the data U_d , E_d , X_d are utilized to form the Hankel matrices by Definition 3. These matrices are further partitioned into two parts, corresponding to the trajectory data in the past

$T_{\text{ini}} \in \mathbb{N}$ steps and the trajectory data in the future $N \in \mathbb{N}$ steps, defined as follows:

$$\begin{bmatrix} U_p \\ U_f \end{bmatrix} = \mathcal{H}_L(U_d), \begin{bmatrix} E_p \\ E_f \end{bmatrix} = \mathcal{H}_L(E_d), \begin{bmatrix} X_p \\ X_f \end{bmatrix} = \mathcal{H}_L(X_d), \quad (14)$$

where $L = T_{\text{ini}} + N$, U_p and U_f contain the upper T_{ini} rows and lower N rows of $\mathcal{H}_L(U_d)$, respectively (similarly for E_p and E_f , X_p and X_f).

Note that for the persistently excitation requirement of order $T_{\text{ini}} + N$, it must hold that $T \geq 2(T_{\text{ini}} + N + 2n) - 1$ [12], [13]. This necessary condition indicates that the column number should be larger than the row number in Hankel matrices.

B. Data-Driven Reachable Set Computation

In this paper, we focus on controlling mixed platoons under process noise and external disturbances. To ensure the robustness of the control system, the reachable set technique is introduced.

1) *System Over-Approximation*: For the mixed platoon system (9), multiple models $[A \ B \ H]$ consistent with collected data are considered due to the presence of process noise $w(k)$. Here, we utilize collected data to construct the matrix zonotope set \mathcal{M}_{ABH} to over-approximate all possible system models consistent with the noisy data, as shown below.

Lemma 2: Given the data sequences U_- , E_- , X_- , and X_+ collected from the mixed platoon system (9), assume the process noise $w(k)$ and disturbance $\epsilon(k)$ are bounded by zonotope sets, given by:

$$w(k) \in \mathcal{Z}_w, \quad \epsilon(k) \in \mathcal{Z}_\epsilon. \quad (15)$$

If the matrix $[X_-^\top \ U_-^\top \ E_-^\top]$ is of full row rank, then the set of all possible $[A \ B \ H]$ can be obtained by:

$$\mathcal{M}_{ABH} = (X_+ - \mathcal{M}_w) \begin{bmatrix} X_- \\ U_- \\ E_- \end{bmatrix}^\dagger, \quad (16)$$

which provides a data-driven over-approximation of system dynamics. In (16), \dagger denotes Moore–Penrose pseudoinverse, and $\mathcal{M}_w = \langle C_{\mathcal{M}_w}, [G_{\mathcal{M}_w}^{(1)}, G_{\mathcal{M}_w}^{(2)}, \dots, G_{\mathcal{M}_w}^{(\gamma_{\mathcal{M}_w})}] \rangle$ is a matrix zonotope set resulting from the noise zonotope set \mathcal{Z}_w , with $\gamma_{\mathcal{M}_w} \in \mathbb{N}$ is the number of generator matrices.

Proof: For the mixed platoon system (9), we have

$$X_+ = [A \ B \ H] \begin{bmatrix} X_- \\ U_- \\ E_- \end{bmatrix} + W_-. \quad (17)$$

Since $[X_-^\top \ U_-^\top \ E_-^\top]$ is of full row rank, we have

$$[A \ B \ H] = (X_+ - W_-) \begin{bmatrix} X_- \\ U_- \\ E_- \end{bmatrix}^\dagger. \quad (18)$$

This allows us to use the bound \mathcal{M}_w to obtain (16). Thus, the matrix zonotope \mathcal{M}_{ABH} serves as an over-approximated

set for system models $\begin{bmatrix} A & B & H \end{bmatrix}$, given the existence of process noise. ■

2) *System Decomposition*: Next, the system described in (9) is decoupled into two parts: nominal dynamics and error dynamics, denoted as follows:

$$x_z(k+1) = Ax_z(k) + Bu_z(k) + H\epsilon_z(k), \quad (19a)$$

$$x_e(k+1) = Ax_e(k) + Bu_e(k) + H\epsilon_e(k) + w(k), \quad (19b)$$

where $x_z(k)$, $u_z(k)$, $\epsilon_z(k)$ and $x_e(k)$, $u_e(k)$, $\epsilon_e(k)$ represent the state, control input, and disturbance input of the nominal dynamics system and error dynamics system, respectively. Precisely, we have

$$\begin{cases} x(k) = x_z(k) + x_e(k), \\ u(k) = u_z(k) + u_e(k), \\ \epsilon(k) = \epsilon_z(k) + \epsilon_e(k), \end{cases} \quad (20)$$

with

$$\epsilon_z(k) = 0, \quad \epsilon_e(k) = \epsilon. \quad (21)$$

This decomposition indicates that the noise and disturbance are only considered in the error system, not the nominal one. Recall that A , B , and H in (19) are unknown but belong to \mathcal{M}_{ABH} .

3) *Feedback Control Law for Error Systems*: For the error system (19b), we need to design a feedback control law $K \in \mathbb{R}^{1 \times 2n}$ that stabilizes all possible A and B . We first compute a set \mathcal{M}_{AB} that includes all possible $\begin{bmatrix} A & B \end{bmatrix}$, expressed as follows:

$$\mathcal{M}_{AB} = \mathcal{M}_{ABH} \begin{bmatrix} \mathbb{I}_{2n+1} \\ \mathbb{O}_{1 \times (2n+1)} \end{bmatrix}, \quad (22)$$

where \mathbb{I} and \mathbb{O} denote the unit and zero matrices with appropriate dimensions, respectively. Then, we apply random sampling methods to solve K based on [26, Lemma 7]. Specifically, we obtain a batch $\mathcal{S}_{N_k} = \{(A^{(1)}, B^{(1)}), (A^{(2)}, B^{(2)}), \dots, (A^{(N_k)}, B^{(N_k)})\}$ by sampling \mathcal{M}_{AB} in an i.i.d. manner according to a probability measure \mathbb{P}_{N_k} . Then, we solve the following linear matrix inequality

$$\begin{bmatrix} -P & AP + BZ \\ PA^\top + Z^\top B^\top & -P \end{bmatrix} \prec 0, \quad \forall (A, B) \in \mathcal{S}_{N_k}, \quad (23)$$

in $P \succ 0$ and Z , which yields

$$K = ZP^{-1}. \quad (24)$$

Note that K depends on the choice of \mathcal{S}_{N_k} . The following lemma provides a robustness guarantee for K .

Lemma 3 (Robustness guarantee for K [26]): For accuracy $\varepsilon \in (0, 1)$ and confidence $\delta \in (0, 1)$, let $N_k \geq \frac{5}{\varepsilon} (\ln \frac{4}{\delta} + d \ln \frac{40}{\varepsilon})$ with $d = 4n \log_2 (2e(2n)^2(2n+1))$. Assume that K is computed according to \mathcal{S}_{N_k} , and satisfied that $\rho(A+BK) \leq 1$ for every pair $(A, B) \in \mathcal{S}_{N_k}$. Then, with probability at least $1 - \delta$ we have

$$\mathbb{P}((A, B) \in \mathcal{M}_{AB}, \rho(A+BK) \geq 1) \leq \varepsilon, \quad (25)$$

where ρ is the spectral radius, and $\rho(A+BK) \geq 1$ means that Schur stability is not satisfied.

4) *Error State Reachable Sets*: Based on (15), (16), (19b) and (24), the recursive relation for the error state reachable set can be obtained as follows:

$$\hat{\mathcal{R}}_{k+i+1}^e = \mathcal{M}_{ABH} \left(\hat{\mathcal{R}}_{k+i}^e \times K \hat{\mathcal{R}}_{k+i}^e \times \mathcal{Z}_\epsilon \right) + \mathcal{Z}_w, \quad (26)$$

where $\hat{\mathcal{R}}_{k+i}^e$ is an over-approximated reachable set for the state $x_e(k+i)$ of the error dynamics system.

C. RDdeP-LCC Optimization Formulation

We proceed to design the RDdeP-LCC optimization formulation. The detailed process is described below:

1) *Trajectory Definition*: For each time step k , we define the state trajectory x_{ini} in the past T_{ini} steps and the predicted state trajectory x_z of the nominal system in the next N steps, denoted as follows:

$$\begin{cases} x_{\text{ini}} = \text{col}(x(k-T_{\text{ini}}+1), x(k-T_{\text{ini}}+2), \dots, x(k)), \\ x_z = \text{col}(x_z(k+1), x_z(k+2), \dots, x_z(k+N)). \end{cases} \quad (27)$$

The control input trajectories u_{ini} and u_z , and disturbance input trajectories ϵ_{ini} and ϵ_z in the past T_{ini} steps and future N steps are defined similarly as in (27).

2) *Cost Function*: We utilize the quadratic function $J(x_z, u_z)$ to quantify the control performance by penalizing the states and control inputs, defined as follows:

$$J(x_z, u_z) = \sum_{i=1}^N (\|x_z(k+i)\|_Q^2 + \|u_z(k+i)\|_R^2), \quad (28)$$

where $Q = \text{diag}(\rho_s, \rho_v, \dots, \rho_s, \rho_v) \in \mathbb{R}^{2n \times 2n}$, $R \in \mathbb{R}$ denote weight matrices, with ρ_s and ρ_v denoting the penalties for spacing deviation and velocity deviation, respectively.

3) *Data-Driven Dynamics*: By Lemma 1 and [14, Proposition 2], the data-driven dynamics can be given by

$$\begin{bmatrix} X_p \\ U_p \\ E_p \\ X_f \\ U_f \\ E_f \end{bmatrix} g = \begin{bmatrix} x_{\text{ini}} \\ u_{\text{ini}} \\ \epsilon_{\text{ini}} \\ x_z \\ u_z \\ \epsilon_z \end{bmatrix}. \quad (29)$$

The existence of $g \in \mathbb{R}^{T-T_{\text{ini}}-N+1}$ satisfying (29) implies that x_z , u_z , and ϵ_z form a future trajectory of length N . Note that to ensure the uniqueness of the future trajectory x_z for given x_{ini} , u_{ini} , ϵ_{ini} , u_z , ϵ_z , it is required that $T_{\text{ini}} \geq 2n$ [14].

4) *Constraints*: The safety of the mixed platoon system is ensured by imposing the following constraints:

$$\begin{cases} x(k+i) \in \mathcal{X}, \\ u(k+i) \in \mathcal{U}, \end{cases} \quad (30)$$

where $\mathcal{X} = \{x(k) \in \mathbb{R}^{2n} \mid |x(k)| \leq \mathbf{1}_n \otimes x_{\text{max}}\}$ is the state constraint, with $x_{\text{max}} = [\tilde{s}_{\text{max}}, \tilde{v}_{\text{max}}]^\top$, where \tilde{s}_{max} and \tilde{v}_{max}

are the constraint limits for spacing deviation and velocity deviation, respectively. In the control input constraint $\mathcal{U} = \{u(k) \in \mathbb{R} \mid |u(k)| \leq u_{\max}\}$, u_{\max} denotes the maximum control input for the CAV.

Combining (26) and (30), the constraint set for the nominal system (19a) can be calculated as follows:

$$\begin{cases} \mathcal{X}_z(k+i) = \mathcal{X} - \hat{\mathcal{R}}_{k+i}^e, \\ \mathcal{U}_z(k+i) = \mathcal{U} - K\hat{\mathcal{R}}_{k+i}^e, \end{cases} \quad (31)$$

which yields the constraints for the predicted trajectory of the nominal system, given by:

$$\begin{cases} x_z(k+i) \in \mathcal{X}_z(k+i), \\ u_z(k+i) \in \mathcal{U}_z(k+i). \end{cases} \quad (32)$$

For the future disturbance sequence ϵ_z of the nominal system, recalling (21), we have

$$\epsilon_z(k+i) = 0. \quad (33)$$

5) *RDDeP-LCC Optimization Formulation*: The final optimization problem is formulated as follows to solve the control input for the CAVs:

$$\begin{aligned} \min_{g, u_z, x_z, \sigma} \quad & J(x_z, u_z) + \lambda_g \|g\|_2^2 + \lambda_\sigma \|\sigma\|_2^2 \\ \text{s.t.} \quad & \begin{bmatrix} X_p \\ U_p \\ E_p \\ X_f \\ U_f \\ E_f \end{bmatrix} g = \begin{bmatrix} x_{\text{ini}} \\ u_{\text{ini}} \\ \epsilon_{\text{ini}} \\ x_z \\ u_z \\ \epsilon_z \end{bmatrix} + \begin{bmatrix} \sigma \\ 0 \\ 0 \\ 0 \\ 0 \\ 0 \end{bmatrix}, \end{aligned} \quad (34)$$

(32), (33),

Motivated by the literature [12], [14], we ensure the feasibility of the optimization problem (34) by penalizing g with regularization and introducing a slack variable $\sigma \in \mathbb{R}^{2nT_{\text{ini}}}$ in (29), where $\lambda_g, \lambda_\sigma \geq 0$ denote the regularization coefficients. This regularization is necessary since the real mixed platoon system has nonlinear dynamics, while the data-driven dynamics (29) is only applicable to LTI systems.

Solving (34) yields an optimal control sequence u_z and the predicted state sequence x_z of the nominal system. Then, by

$$\begin{aligned} u(k+1) &= u_z(k+1) + u_e(k+1) \\ &= u_z(k+1) + K(x(k+1) - x_z(k+1)), \end{aligned} \quad (35)$$

where K is calculated from (24), we obtain the final control input for the CAV.

Remark 2: It is worth noting that in (34), $x_{\text{ini}}, u_{\text{ini}}, \epsilon_{\text{ini}}$ represent the past trajectories of the actual system (9), while x_z, u_z, ϵ_z denote the predicted trajectories of the nominal system (19a). As shown in (21), we assume $\epsilon_z = 0$, and capture the actual disturbance $\epsilon_e = \epsilon$ solely in the error system (19b). Provided $\epsilon(k) \in \mathcal{Z}_\epsilon$ in (15), the disturbance effect is further incorporated into the calculation of the error reachable set (26), resulting in a more stringent constraint (32) on x_z and u_z of the nominal system. This approach addresses the influence

of process noise and unknown future disturbances, which are neglected in the standard DeeP-LCC [14].

IV. SIMULATION RESULTS

In this section, we carry out nonlinear traffic simulations to verify the performance of the proposed RDDeP-LCC method.

A. Simulation Setup

For the mixed platoon system depicted in Fig. 1, we set the platoon size as $n = 3$. The dynamics of vehicles are described in (3). For HDVs, we utilize the OVM model [25] to describe its car-following behaviors, with the specific model and the parameter selection presented in [3]. The parameters of the RDDeP-LCC in the simulation are set as follows:

- For offline data collection, near the equilibrium state $v^* = 15$ m/s, we utilize a random control input within $[-0.2, 0.2]$ for the CAVs and apply a random disturbance within $[-0.5, 0.5]$ to the head vehicle's velocity. Then the offline pre-collected trajectories of length $T = 1000$ with a sampling interval of 0.1 s are used to construct (10)-(14). Based on the pre-collected data sequences, \mathcal{M}_{ABH} can be obtained using (16), and K is computed using Lemma 3 with $\varepsilon = 0.01$ and $\delta = 0.001$.
- For online predictive control, the past sequence length $T_{\text{ini}} = 20$ and the future sequence length $N = 5$ are selected in (27). For the cost function (28), the coefficients are set to $\rho_s = 0.5$, $\rho_v = 1$, and $R = 0.1$. We set $x_{\max} = [7, 7]^T$ and $u_{\max} = 5$ in the constraints (30). In the optimization formulation (34), the parameters are set to $\lambda_g = 10$ and $\lambda_\sigma = 10$. Based on the localization requirements for local roads in the United States [27], we set the range of bounded process noise is $|w(k)| \leq 0.05$.

In addition, we choose standard MPC with knowledge of system dynamics (9) and standard DeeP-LCC with the same pre-collected data as baseline methods. All shared parameters of standard MPC and DeeP-LCC have the same values as those of RDDeP-LCC, except for $N = 20$ in DeeP-LCC, which follows the setup in [14].

In order to quantify the performance, this paper adopts the velocity mean absolute deviation R_m and velocity standard deviation R_s as performance indices, given by:

$$R_m = \frac{1}{T_s} \frac{1}{n} \sum_{t=0}^{T_s} \sum_{i=1}^n |v_i(t) - v^*|, \quad (36a)$$

$$R_s = \sqrt{\frac{1}{T_s} \frac{1}{n} \sum_{t=0}^{T_s} \sum_{i=1}^n (v_i(t) - v^*)^2}, \quad (36b)$$

where T_s is the total simulation time.

B. Simulation Results

1) *Simulation A (Near Equilibrium State)*: To reproduce a traffic wave scenario, inspired by [7], [14], we introduce a sinusoidal disturbance with an amplitude of 4 m/s and a period of 10 s on the head vehicle. The velocity profiles of our proposed approach and other baseline methods are

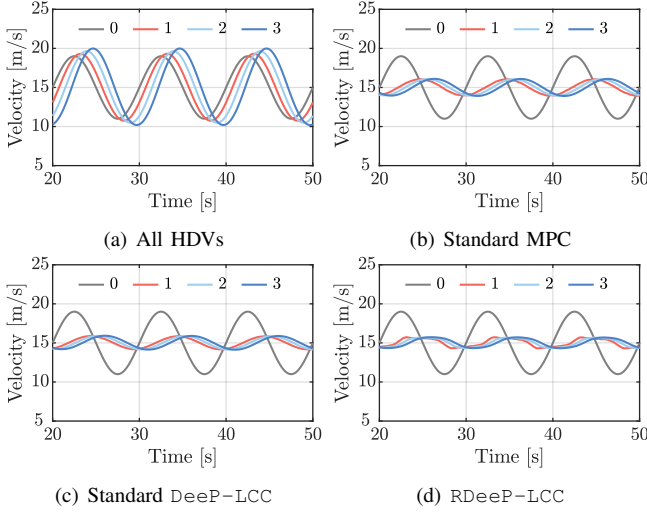


Fig. 3. Velocity profiles under different control methods for Simulation A. The gray profile, the red profile, and the blue profiles represent the head vehicle (indexed 0), the CAV (indexed 1), and the HDVs (indexed 2, 3), respectively. Note that DeeP-LCC and RDDeeP-LCC use the same dataset.

TABLE I
THE R_m AND R_s IN SIMULATION A

Index	All HDVs	MPC	DeeP-LCC	RDDeeP-LCC
R_m	2.412 (—)	0.673 (↓ 72.1 %)	0.511 (↓ 78.8 %)	0.486 (↓ 79.9 %)
R_s	2.892 (—)	0.747 (↓ 74.2 %)	0.553 (↓ 80.9 %)	0.530 (↓ 81.7 %)

shown in Fig. 3. From Fig. 3(a), it is evident that the perturbation is amplified during propagation when all vehicles are HDVs. Conversely, when CAVs utilize standard MPC, standard DeeP-LCC, or RDDeeP-LCC, as shown in Fig. 3(b)-(d), respectively, the magnitude of the perturbation is notably reduced. This demonstrates the capability of the CAVs to mitigate undesired disturbances when employing either of the three methods.

Note that different pre-collected data may affect the data-driven controller's performance due to the existence of process noise. To further qualitatively compare the performance, we collect 20 random data sets with a consistent length of $T = 1000$ to construct the Hankel matrices (14). We then conduct simulations using these data sets and analyze the performance indices (36a) and (36b). The results, presented in Table I, indicate that our RDDeeP-LCC approach exhibits the smallest mean values of (36a) and (36b) compared to the baseline methods. Specifically, compared to the cases of all HDVs, our approach achieves average reductions of 79.9% and 81.7%, while the baseline methods achieve less reductions. This reveals the superior performance of our approach in suppressing undesired traffic oscillations, as higher values of R_m and R_s indicate a larger velocity fluctuation and a weaker wave-dampening ability of the CAVs' controller.

2) *Simulation B (Standard Test Cycle)*: Inspired by the experiments conducted in [14], we devise a comprehensive

TABLE II
THE R_m AND R_s IN SIMULATION B

Index	All HDVs	MPC	DeeP-LCC	RDDeeP-LCC
R_m	0.566 (—)	0.537 (↓ 5.1 %)	0.620 (↑ 9.5 %)	0.526 (↓ 7.1 %)
R_s	0.889 (—)	0.785 (↓ 11.7 %)	0.948 (↑ 6.6 %)	0.778 (↓ 12.5 %)

acceleration and deceleration scenario based on the New European Driving Cycle (NEDC) to assess the effectiveness of the proposed RDDeeP-LCC in enhancing platoon performance. In this scenario, We adopt the ECE Elementary Urban Cycle (Part One of the Urban Driving Cycle) as a trajectory for the head vehicle. It is noteworthy that, in simulation B, we assume the real-time velocity of the head vehicle as the equilibrium velocity for online predictive control.

The simulation results depicted in Fig. 4 reveal the performance of mixed platoons using different control methods. Overall, the platoons successfully track the desired trajectory for all the three methods. However, there are instances, such as at about 65 s and 145 s, where both All HDVs and DeeP-LCC exhibit noticeable overshoot, as depicted in the insets of Fig. 4(a),(c). In contrast, both standard MPC and RDDeeP-LCC effectively mitigate overshoot, resulting in superior tracking performance in these cases, as illustrated in the insets of Fig. 4(b),(d). This highlights the robustness and effectiveness of RDDeeP-LCC in achieving precise control under time-varying traffic conditions.

Table II illustrates the R_m and R_s indices, which provide straightforward insights into the control performance in terms of velocity errors. It is observed that the proposed RDDeeP-LCC method shows the best performance compared to all other cases. It is worth noting that the standard DeeP-LCC shows the highest values for R_m and R_s . This means that under the influence of process noise and disturbances, the data-driven predictive control methods without explicit robust design could have unsatisfactory tracking performance, which could be even worse than HDV's natural behaviors in traffic flow with time-varying equilibrium states. In contrast, our proposed method enhances robustness against process noise and disturbances for mixed platoon control.

V. CONCLUSIONS

In this paper, we have proposed RDDeeP-LCC for mixed platoon control to address the existence of noise and disturbances by combining data-driven reachable set analysis and the standard data-enabled predictive control framework. Traffic simulation results have demonstrated that our method effectively reduces undesired traffic waves and achieves excellent tracking performance compared to all HDVs, standard MPC, and standard DeeP-LCC. Future directions include investigating mixed platoon control under communication delays and experimental validations with real human drivers in the loop.

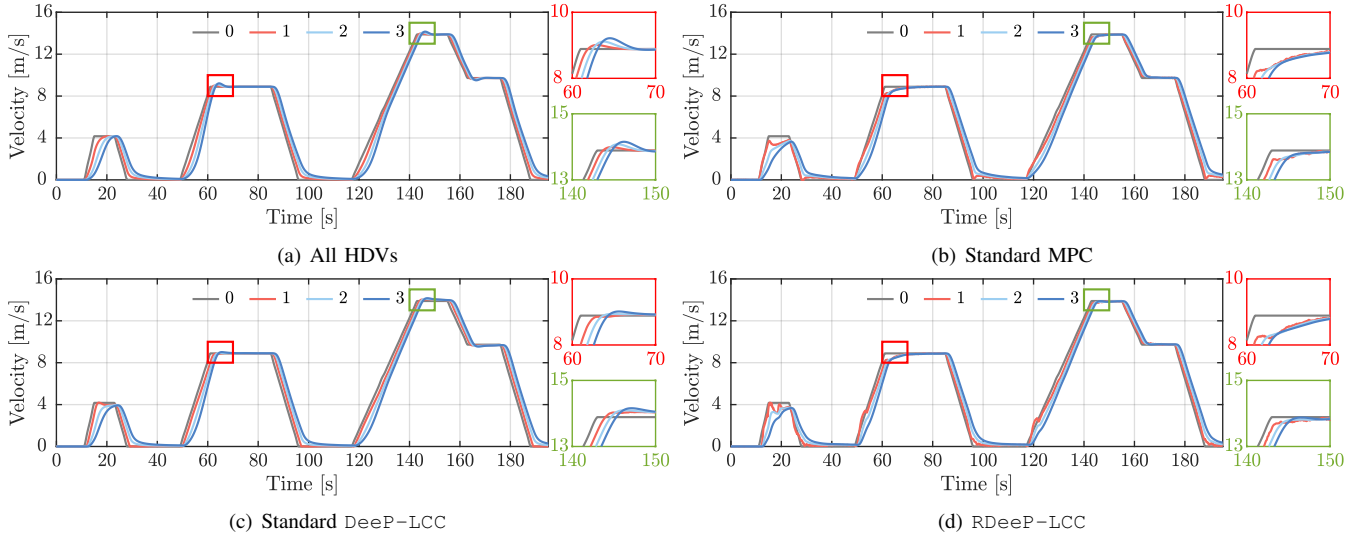


Fig. 4. Velocity profiles under different control methods for Simulation B. The graphs are colored corresponding to the color of profiles in Fig. 3.

REFERENCES

- [1] J. Guanetti, Y. Kim, and F. Borrelli, "Control of connected and automated vehicles: State of the art and future challenges," *Annual reviews in control*, vol. 45, pp. 18–40, 2018.
- [2] M. Hu, J. Li, Y. Bian, J. Wang, B. Xu, and Y. Zhu, "Distributed coordinated brake control for longitudinal collision avoidance of multiple connected automated vehicles," *IEEE Transactions on Intelligent Vehicles*, vol. 8, no. 1, pp. 745–755, 2022.
- [3] J. Wang, Y. Zheng, Q. Xu, J. Wang, and K. Li, "Controllability analysis and optimal control of mixed traffic flow with human-driven and autonomous vehicles," *IEEE Transactions on Intelligent Transportation Systems*, vol. 22, no. 12, pp. 7445–7459, 2021.
- [4] S. Li, H. Zheng, J. Wang, C. Chen, Q. Xu, J. Wang, and K. Li, "Information flow topology in mixed traffic: A comparative study between "looking ahead" and "looking behind,"" in *2023 IEEE 26th International Conference on Intelligent Transportation Systems (ITSC)*. IEEE, 2023, pp. 5675–5681.
- [5] C. Wu, A. R. Kreidieh, K. Parvate, E. Vinitsky, and A. M. Bayen, "Flows: A modular learning framework for mixed autonomy traffic," *IEEE Transactions on Robotics*, vol. 38, no. 2, pp. 1270–1286, 2021.
- [6] J. Wang, Y. Zheng, C. Chen, Q. Xu, and K. Li, "Leading cruise control in mixed traffic flow: System modeling, controllability, and string stability," *IEEE Transactions on Intelligent Transportation Systems*, vol. 23, no. 8, pp. 12 861–12 876, 2022.
- [7] I. G. Jin and G. Orosz, "Optimal control of connected vehicle systems with communication delay and driver reaction time," *IEEE Transactions on Intelligent Transportation Systems*, vol. 18, no. 8, pp. 2056–2070, 2016.
- [8] S. Feng, Z. Song, Z. Li, Y. Zhang, and L. Li, "Robust platoon control in mixed traffic flow based on tube model predictive control," *IEEE Transactions on Intelligent Vehicles*, vol. 6, no. 4, pp. 711–722, 2021.
- [9] C. Zhao, H. Yu, and T. G. Molnar, "Safety-critical traffic control by connected automated vehicles," *Transportation research part C: emerging technologies*, vol. 154, p. 104230, 2023.
- [10] M. Huang, Z. Jiang, and K. Ozbay, "Learning-based adaptive optimal control for connected vehicles in mixed traffic: robustness to driver reaction time," *IEEE transactions on cybernetics*, vol. 52, no. 6, pp. 5267–5277, 2020.
- [11] L. Hewing, K. P. Wabersich, M. Menner, and M. N. Zeilinger, "Learning-based model predictive control: Toward safe learning in control," *Annual Review of Control, Robotics, and Autonomous Systems*, vol. 3, pp. 269–296, 2020.
- [12] J. Coulson, J. Lygeros, and F. Dörfler, "Data-enabled predictive control: In the shallows of the DeePC," in *2019 18th European Control Conference (ECC)*. IEEE, 2019, pp. 307–312.
- [13] J. C. Willems, P. Rapisarda, I. Markovsky, and B. L. De Moor, "A note on persistency of excitation," *Systems & Control Letters*, vol. 54, no. 4, pp. 325–329, 2005.
- [14] J. Wang, Y. Zheng, K. Li, and Q. Xu, "DeeP-LCC: Data-enabled predictive leading cruise control in mixed traffic flow," *IEEE Transactions on Control Systems Technology*, vol. 31, no. 6, pp. 2760–2776, 2023.
- [15] J. Wang, Y. Zheng, J. Dong, C. Chen, M. Cai, K. Li, and Q. Xu, "Implementation and experimental validation of data-driven predictive control for dissipating stop-and-go waves in mixed traffic," *IEEE Internet of Things Journal*, vol. 11, no. 3, pp. 4570–4585, 2023.
- [16] C. Zhao and H. Yu, "Robust safety for mixed-autonomy traffic with delays and disturbances," *arXiv preprint arXiv:2310.04007*, 2023.
- [17] L. Huang, J. Zhen, J. Lygeros, and F. Dörfler, "Robust data-enabled predictive control: Tractable formulations and performance guarantees," *IEEE Transactions on Automatic Control*, vol. 68, no. 5, pp. 3163–3170, 2023.
- [18] J. Berberich, J. Köhler, M. A. Müller, and F. Allgöwer, "Data-driven model predictive control with stability and robustness guarantees," *IEEE Transactions on Automatic Control*, vol. 66, no. 4, pp. 1702–1717, 2020.
- [19] X. Shang, J. Wang, and Y. Zheng, "Smoothing mixed traffic with robust data-driven predictive control for connected and autonomous vehicles," *arXiv preprint arXiv:2310.00509*, 2023.
- [20] B. Schürmann, M. Klischat, N. Kochdumper, and M. Althoff, "Formal safety net control using backward reachability analysis," *IEEE Transactions on Automatic Control*, vol. 67, no. 11, pp. 5698–5713, 2021.
- [21] Q. Xu, Y. Liu, J. Pan, J. Wang, J. Wang, and K. Li, "Reachability analysis plus satisfiability modulo theories: An adversary-proof control method for connected and autonomous vehicles," *IEEE Transactions on Industrial Electronics*, vol. 70, no. 3, pp. 2982–2992, 2022.
- [22] J. Lan, D. Zhao, and D. Tian, "Data-driven robust predictive control for mixed vehicle platoons using noisy measurement," *IEEE Transactions on Intelligent Transportation Systems*, vol. 24, no. 6, pp. 6586–6596, 2023.
- [23] A. Alanwar, A. Koch, F. Allgöwer, and K. H. Johansson, "Data-driven reachability analysis from noisy data," *IEEE Transactions on Automatic Control*, 2023.
- [24] M. Althoff, "Reachability analysis and its application to the safety assessment of autonomous cars," Ph.D. dissertation, Technische Universität München, 2010.
- [25] M. Bando, K. Hasebe, A. Nakayama, A. Shibata, and Y. Sugiyama, "Dynamical model of traffic congestion and numerical simulation," *Physical review E*, vol. 51, no. 2, p. 1035, 1995.
- [26] A. Russo and A. Proutiere, "Tube-based zonotopic data-driven predictive control," in *2023 American Control Conference (ACC)*. IEEE, 2023, pp. 3845–3851.
- [27] T. G. Reid, S. E. Houts, R. Cammarata, G. Mills, S. Agarwal, A. Vora, and G. Pandey, "Localization requirements for autonomous vehicles," *SAE International Journal of Connected and Automated Vehicles*, vol. 2, no. 12-02-03-0012, pp. 173–190, 2019.